Magnetic activity at infrared frequencies in structured metallic photonic crystals

2002 J. Phys.: Condens. Matter 14 6383

(http://iopscience.iop.org/0953-8984/14/25/307)

INSTITUTE OF PHYSICS PUBLISHING JOURNAL OF PHYSICS: CONDENSED MATTER

J. Phys.: Condens. Matter **14** (2002) 6383–6394 PII: S0953-8984(02)36131-9

Magnetic activity at infrared frequencies in structured metallic photonic crystals

S O'Brien and J B Pendry

Condensed Matter Theory Group, The Blackett Laboratory, Imperial College, London SW7 2BZ, UK

E-mail: s.obhriain@ic.ac.uk

Received 23 April 2002
Published 14 June 2002
Online at stacks.iop.org/JPhysCM/14/6383

Abstract

We derive the effective permeability and permittivity of a nanostructured metallic photonic crystal by analysing the complex reflection and transmission coefficients for slabs of various thicknesses. These quantities were calculated using the transfer matrix method. Our results indicate that these structures could be used to realize a negative effective permeability, at least up to infrared frequencies. The origin of the negative permeability is a resonance due to the internal inductance and capacitance of the structure. We also present an analytic model for the effective permeability of the crystal. The model reveals the importance of the inertial inductance due to the finite mass of the electrons in the metal. We find that this contribution to the inductance has implications for the design of metallic magnetic structures in the optical region of the spectrum. We show that the magnetic activity in the structure is accompanied by the concentration of the incident field energy into very small volumes within the structure. This property will allow us to considerably enhance non-linear effects with minute quantities of material.

1. Introduction

Composite electromagnetic materials can be considered as effectively homogeneous media when the structure varies spatially on a scale much less than the incident radiation. A set of effective response functions ϵ_{eff} and/or μ_{eff} can then be ascribed to these materials. By microstructuring metallic elements, materials with striking electromagnetic properties which were previously unattainable have now been tested in the GHz and RF ranges.

For example, a variety of structures have been proposed which are characterized by an effective permeability of the form

$$\mu_{eff} = 1 - \frac{f\omega^2}{\omega^2 - \omega_0^2 + \mathrm{i}\Gamma\omega}. \tag{1}$$

0953-8984/02/256383+12$30.00

Here f is the filling fraction in the unit cell of the material and in the absence of losses ($\Gamma \to 0$) the effective permeability diverges at the resonance frequency ω_0. Structures composed of metallic elements which display a magnetic response as above include split-ring resonators and the so-called Swiss-roll structure [1, 2]. These structures are resonant because of an internal capacitance and inductance within each element. Note that these structures now provide the possibility of observing a negative effective permeability over a finite frequency range in the absence of any intrinsically magnetic material in the structure.

By constraining the electrons to run along thin wires arranged in a three-dimensional lattice we can create structures with a dielectric dispersion characteristic of a plasma:

$$\epsilon_{eff} = 1 - \frac{\omega_p^2}{\omega^2}. \tag{2}$$

The plasma frequency ω_p can be reduced into the infrared or microwave region of the spectrum simply by varying the concentration and thickness of the wires which form the lattice [3]. Once the frequency is less than the plasma frequency, the effective permittivity is negative.

By combining these thin wire structures with resonant magnetic structures the material can be tuned such that both the effective permittivity and effective permeability are simultaneously negative. A so-called left-handed material then results with many novel electromagnetic properties [4, 5]. For example, at a single frequency where $\epsilon_{eff} = \mu_{eff} = -1$, a parallel-sided slab of the material will focus all the Fourier components of an image, both radiative and evanescent. This phenomenon of perfect lensing thus allows for improved near-field imaging potential [6].

The zeroth-order Mie resonance in dielectric particles represents an alternative to metallic implementations of the above magnetic response [7]. In that study an array of cylinders of large dielectric constant was considered and it was found that a negative permeability could be realized. Low-loss ferroelectric materials make the large dielectric constants possible at the frequencies considered, a few GHz. While the magnetic response was found to be potentially large in this instance, such large dielectric constants are not to be found at present at higher frequencies.

In this paper we demonstrate that a metallic split ring can be used to implement a magnetic response, including a negative effective permeability, in principle up to infrared frequencies. The nanostructured crystal that we consider represents an adaptation of the split-ring configuration for operation at higher frequencies in that we have again incorporated a large capacitance into the structure, thus allowing a current to flow in the absence of a continuous conducting path in the xz-plane. Since the structure is essentially a single metallic ring which has been split symmetrically, it is likely to be more easily fabricated at submicron scales than the two concentric rings considered in [1]. As for the structures considered previously we will require that the length scales determined by the unit-cell dimension and the free-space wavelength at the resonance frequency are well separated. This allows us to sensibly speak of an effective permeability and permittivity for the crystal.

As was the case with the original split-ring structure [1], we find that the magnetic activity implies that there are regions in the structure where local field strengths can be many orders of magnitude larger than in free space. Thus there exists considerable potential for enhancing non-linear effects.

2. A magnetic nanostructure

The two-dimensional unit cell which we consider is shown in figure 1(b). It consists of a square silver column which we have structured on a nanometre scale in order to define an internal

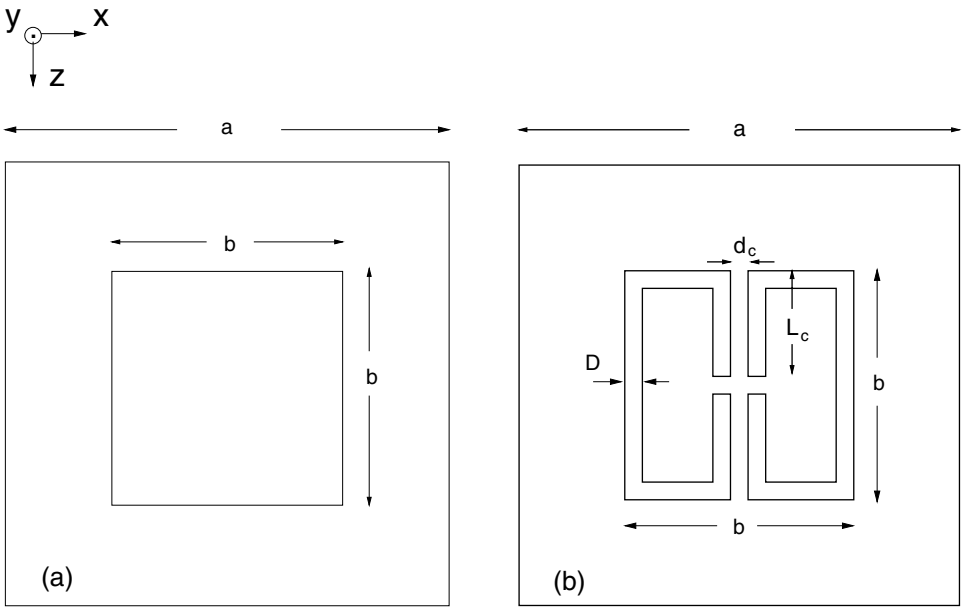

Figure 1. Two-dimensional unit cells of the structures considered. The unit-cell dimension is a in both cases. (a) A solid silver column with filling fraction b^2/a^2. (b) The magnetic nanostructure composed of silver and with the same filling fraction as in (a). The thickness of the metal films is D. Each capacitance is defined by a separation d_c and a length L_c. The results presented here are for incident waves propagating along the z-direction.

inductance and capacitance, thus forming a resonant structure. The unit cell is also square with a side length a which we take to be 600 nm. The metallic sheets are of uniform thickness D while separations d_c and lengths L_c define the capacitance in the structure as shown. The polarization of the incident light which is of interest here is that for which the magnetic field is oriented parallel to the axis of the column along the y-direction (p polarization).

At the frequencies we consider here, the dielectric response of bulk silver is dominated by the plasma-like behaviour of the electron gas. It can be described by a complex dielectric function of the form

$$\tilde{\epsilon}(\omega) = (\epsilon_1, \epsilon_2) = \epsilon_\infty - \frac{\omega_p^2}{\omega(\omega + \mathrm{i}\gamma)}. \tag{3}$$

Thus the displacement current dominates in this high-frequency region and for $\omega_p \gg \omega \gg \gamma$, $\tilde{\epsilon}$ is essentially a large negative real number. Here we will use the empirical values $\epsilon_\infty = 5.7$, $\omega_p = 9.013$ eV and $\gamma = 0.018$ eV.

In figure 2 we have plotted the photonic band structure for a square lattice of the resonators of figure 1(b) and for p-polarized waves against the frequency. We have also included the photonic band structure for a square lattice of solid silver columns as shown in figure 1(a). In each case the unit-cell length a is 600 nm and the length b, which defines the filling fraction, is 312 nm. For the resonators we have used $L_c = 144$ nm and $d_c = D = 24$ nm. These band structures were calculated using the transfer matrix method [8]. The scaled wavevector is the quantity $\beta a/\pi$, where β is the Bloch wavevector for the infinite system. For comparison, we have also included the free light dispersion on this scale. In the case of the solid columns we find the familiar linear dispersion of wavevector with frequency up to a band gap due to Bragg scattering in the crystal where $\omega \simeq \pi c/a$ (not shown). Away from the position of the

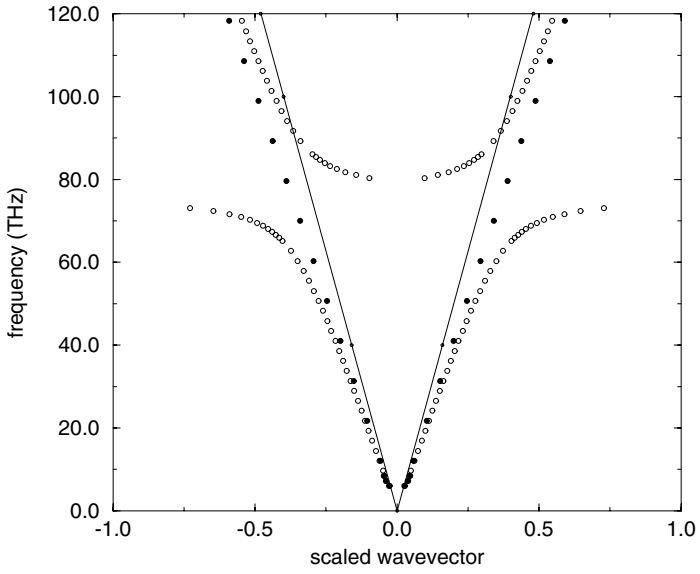

Figure 2. Photonic band structure for p polarization of a square lattice of the magnetic structures (open circles) and for the solid silver columns (filled circles). The free light dispersion is the solid line. The dimensions defining these structures are $a = 600$ nm, $b = 312$ nm, $L_c = 144$ nm and $d_c = D = 24$ nm.

resonance at ≈75 THz, the band structure of the nanostructured resonators is also characterized by the same linear dispersion. Thus we can be confident that we are operating in the effective medium regime for these structures.

As figure 2 demonstrates, a gap has been introduced into the dispersion relationship above the position of the resonance where no propagating modes are allowed in the crystal. In an effective medium picture the refractive index is therefore imaginary and hence either ϵ_{eff} or μ_{eff} has a negative real part.

Since our filling fraction is not too large, we can make an estimate of the resonance frequency for this structure by considering the geometrical inductance and capacitance of the individual element. We take the geometrical inductance per unit length of the structure, L_g, to be given by the area enclosed by the resonator: $L_g = \mu_0(b - 2D)^2$. The capacitance per unit length of the structure for series connection is given by $C = \epsilon_0 L_c/2d_c$. Circuit theory then predicts a resonance frequency $\omega_0 = (L_g C)^{-1/2} \simeq 104$ THz. Note that we have neglected the contribution to the inductance of the structure provided by the electrons in the metal. A simple model for the effective permeability of these structures which we present later will demonstrate that consideration of the geometrical inductance of the structure alone leads us to overestimate the resonance frequency.

3. Determination of the effective permeability

Our aim is to characterize the electromagnetic properties of the system in terms of an effective permittivity, ϵ_{eff}, and permeability, μ_{eff}. For homogeneous media, knowledge of the refractive index n and wave impedance z allows us to find ϵ_{eff} and μ_{eff} using

$$\epsilon_{eff} = n/z \qquad \text{and} \qquad \mu_{eff} = nz. \tag{4}$$

Again using the transfer matrix method we can calculate the (complex) reflection and transmission coefficients for waves normally incident on a slab of the crystal. Analytic expressions for these quantities, assuming a homogeneous medium, can then be inverted to determine n and z.

The complex transmission and reflection coefficients are given by

$$t^{-1} = [\cos x - \mathrm{i}\cosh u \sin x]\mathrm{e}^{\mathrm{i}kd_s}, \tag{5}$$

and

$$r = -[\mathrm{i}t \sinh u \sin x]\mathrm{e}^{\mathrm{i}kd_s}, \tag{6}$$

respectively, where $x \equiv nkd_s$ and $u \equiv \log z$, $k = \omega/c$ is the incident wavenumber and d_s is the width of the slab considered which we take to be the unit-cell length times the number of cells in the propagation direction. Inverting these equations we find that

$$\cos(nkd_s) = \frac{1 - r^2 + t^2}{2t}, \tag{7}$$

and

$$z = \alpha \pm \sqrt{\alpha^2 - 1}, \tag{8}$$

where

$$\alpha = \frac{1 + r^2 - t^2}{\sqrt{[1 - (r^2 - t^2)]^2 - 4t^2}}. \tag{9}$$

These equations define complex multi-branched functions, but additional knowledge of the system and results for more than one thickness of sample can be used to determine the correct values unambiguously [9].

In figure 3 we have plotted the reflectance ('R'), transmittance ('T') and absorbance ('A'), for two and for four layers of the structure. These are also the numbers of layers which we use to determine the refractive index and impedance of the structure. Note how the transmittance is close to zero above the resonance for as little as two layers, indicating the strong attenuation of the incident wave inside the crystal. As a consequence of the large surface area in each unit cell, the absorbance is also relatively large near the resonance where the radiation is interacting strongly with the structure.

The refractive index and impedance that we derived for the structure are given in figure 4. As expected, the refractive index and impedance are both large near the resonance frequency, and are primarily imaginary in the band-gap region.

The calculated effective permittivity and permeability are given in figure 5. We see that the gap in the dispersion relationship plotted in figure 2 is due to an effective negative permeability. Note the dispersion in the effective permittivity with frequency. Its form is similar to that which was found in [7] with an anomalous negative sign of the imaginary part.

By increasing the capacitance in the structure we were able to confirm that this behaviour is symptomatic of the finite wavevector and consequent coupling of the electric and magnetic fields at the level of the unit cell. An increasing capacitance, for fixed unit-cell dimension and filling fraction, increases the separation between the length scales defining the unit cell and the free-space wavelength at the resonance frequency. We found that this results in a reduced level of dispersion in the dielectric response of the crystal while leaving the magnetic response essentially unchanged.

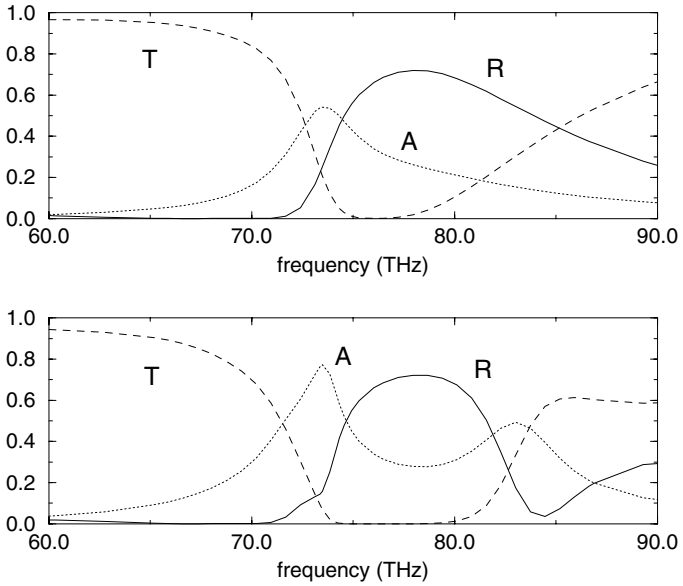

Figure 3. Reflectance, transmittance and absorbance for two layers of the magnetic structure (top) and four layers (bottom). The reflectance is the solid curve, the transmittance is the dashed curve and the dotted curve is the absorbance in each case. The dimensions defining the magnetic structure are as for figure 2.

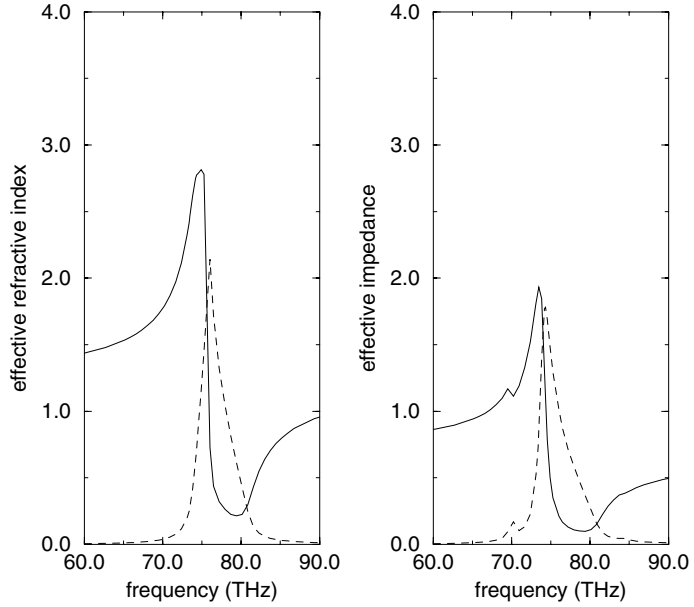

Figure 4. The calculated effective refractive index (left) and effective impedance (right) of the magnetic structure. The solid curves are the real parts and the dashed curves are the imaginary parts in each case. The dimensions defining the magnetic structure are as for figure 2.

4. Scaling of the magnetic response with the unit-cell dimension

We have demonstrated that, with suitable adaptations, the range of operation of the split-ring resonators can be extended into the infrared region of the spectrum. An interesting question

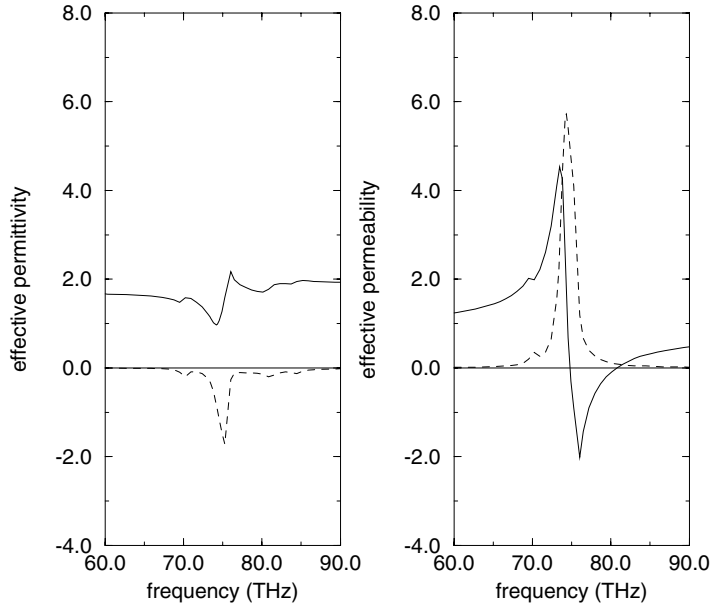

Figure 5. The calculated effective permittivity (left) and permeability (right) of the magnetic structure. The solid curves are the real parts and the dashed curves are the imaginary parts in each case. The dimensions defining the magnetic structure are as for figure 2.

Table 1. Scaled dimensions, in nanometres, of the magnetic structure of figure 1(b). The corresponding effective permeability in each case is given in figure 6.

a	b	D	L_c	d_c
600	312	24	144	24
300	156	12	72	12
150	78	6	36	6

to ask is whether we can push the frequency of operation into the near-infrared or even the visible spectrum, simply by making the structures smaller in size. To answer this we took the structure whose effective response functions are given in figure 5 and examined how the response scales as the unit-cell dimension is reduced.

The results are given in figure 6 where we have plotted the effective permeability of the structure for a unit-cell dimension $a = 600$ nm as before and for $a = 300$ and 150 nm. Thus each of the dimensions defining the structure is halved as the unit cell becomes smaller. Considering the structure as a series LC circuit containing the magnetic inductance and capacitance alone, we would expect the resonance frequency to double each time the unit-cell length is halved. However, we see that the scaling behaviour is very different and in fact the resonances become closer together in frequency as a is decreased.

To explain the origin of this behaviour we can use a simple physical model to derive an expression for the effective permeability of the crystal in the limit where the free-space wavelength $\lambda_0 \gg R$, the internal radius of the structure as shown in figure 7(a).

We apply a time-varying magnetic field H_{ext} along the axis of the structure. Voltages will be induced around its circumference according to $\nabla \times E = -\partial_t B_{int}$, where B_{int} is the magnetic induction inside the structure. The displacement current per unit length is $J_\phi = d\,\partial_t D_\phi$ where

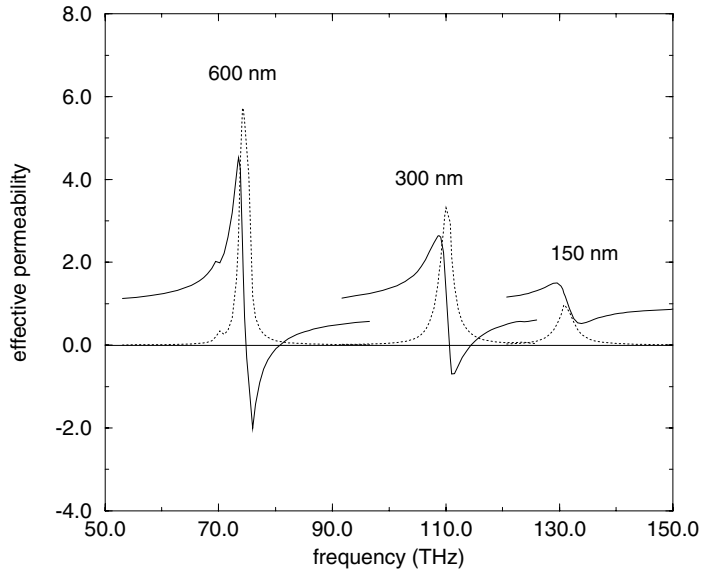

Figure 6. Scaling of the effective permeability of the magnetic structure as the unit-cell dimension and the dimensions of the structure are uniformly decreased. The labelling in each case gives the unit-cell dimension a. The dimensions of each structure, in nanometres, are given in table 1. In each case, the solid curves are the real parts and the dotted curves are the imaginary parts.

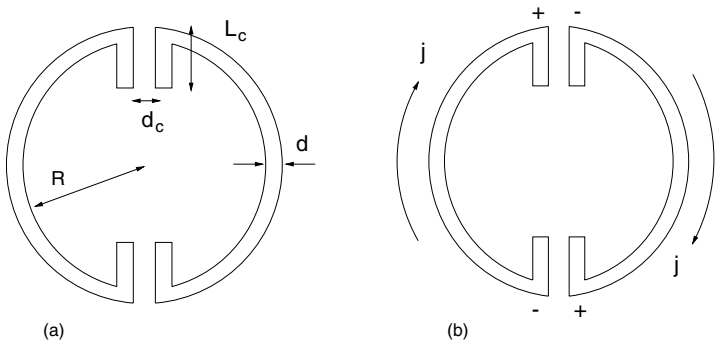

Figure 7. (a) The circular metallic resonator which we consider for our model calculation of the effective permeability. The internal radius of the structure is R; the thickness of the silver film is d. As before, the capacitance in the structure is defined by a separation d_c and a length L_c. (b) An illustration of the induced displacement currents j and charges which give rise to the magnetic response of the structure.

we have assumed that the thickness of the metal film is much less than the skin depth in the metal, δ, which is $\approx$22 nm in the region of frequency considered here. Using the Ampère law to relate the fields inside and outside of the structure, it is straightforward to show that

$$\frac{H_{int}}{H_{ext}} = \left[1 - \frac{\omega\mu_0\pi R^2}{\frac{2\pi R}{\omega\epsilon_0\tilde{\epsilon}d} + \frac{2d_c}{\omega\epsilon_0 L_c}}\right]^{-1}. \tag{10}$$

Now consider a square array of these structures in vacuum with filling fraction f. Since the magnetic fields are everywhere parallel to the boundaries of the structure, the homogenization

Table 2. Dimensions of the magnetic structure of figure 1(b), and the corresponding dimensions of the circular structure of figure 7 which we use to calculate the effective permeability as plotted in figure 8. All dimensions are in nanometres. The dimensions L_c and d_c for both sets of structures are given in table 1.

a	b	D	R	d
600	312	24	161.4	14.6
300	156	12	78.8	9.2
150	78	6	38.7	5.3

law gives for the effective permeability

$$H_{ext}\tilde{\mu}_{eff} = (1 - f)H_{ext} + f H_{int}. \tag{11}$$

Using equations (10) and (11) and assuming that $\tilde{\epsilon} \simeq -\omega_p^2/\omega(\omega + \mathrm{i}\gamma)$, we can write $\tilde{\mu}_{eff}$ in the familiar resonant form of

$$\tilde{\mu}_{eff} = 1 - \frac{f'\omega^2}{\omega^2 - \omega_0'^2 + \mathrm{i}\Gamma\omega}, \tag{12}$$

where

$$f' = \frac{L_g}{L_g + L_i} f, \tag{13}$$

$$\omega_0'^2 = (L_g + L_i)^{-1} C^{-1}, \tag{14}$$

and

$$\Gamma = \frac{L_i}{L_g + L_i}\gamma. \tag{15}$$

In the above expressions $L_g = \mu_0 \pi R^2$ is the geometrical inductance of the structure. We see that the resonance occurs at a lower frequency than that given by $(L_g C)^{-1/2}$ because of an additional inductive impedance in the structure, $L_i = 2\pi R/\epsilon_0 \omega_p^2 d$, that arises from the finite electron mass. This can be seen by examining the expression for the plasma frequency in the bulk metal which determines the conductivity:

$$\omega_p^2 = \frac{ne^2}{\epsilon_0 m_e}. \tag{16}$$

Thus on taking the limit $m_e \to 0$, the imaginary part of the conductivity becomes infinite, in which case $L_i \to 0$. The damping of the resonance according to this model is determined by the relation between the two contributions to the inductance of the structure. As the dimensions of the structure are reduced, that fraction of the energy of the displacement current associated with the inertial mass of the electrons increases. For finite γ, dissipative losses in the metal then increase.

In order to compare the predictions of our model with the results of transfer matrix simulations given in figure 6 we use the same values of L_c and d_c in each case. For the internal radius, R, of the structure we set $\pi(R + d)^2 = b^2$ and, in order to reflect the fact that the fields decay exponentially in the film, we also set $d = \int_0^D \exp(-z/\delta)\,\mathrm{d}z$. The resulting dimensions of the structure in each case are given in table 2. All dimensions are given in nanometres.

The results are given in figure 8 where we see that, although the shift of the resonance frequency to a lower value than that given by $(L_g C)^{-1/2}$ is not as dramatic, the model can qualitatively predict the scaling behaviour that we observed in our transfer matrix calculations.

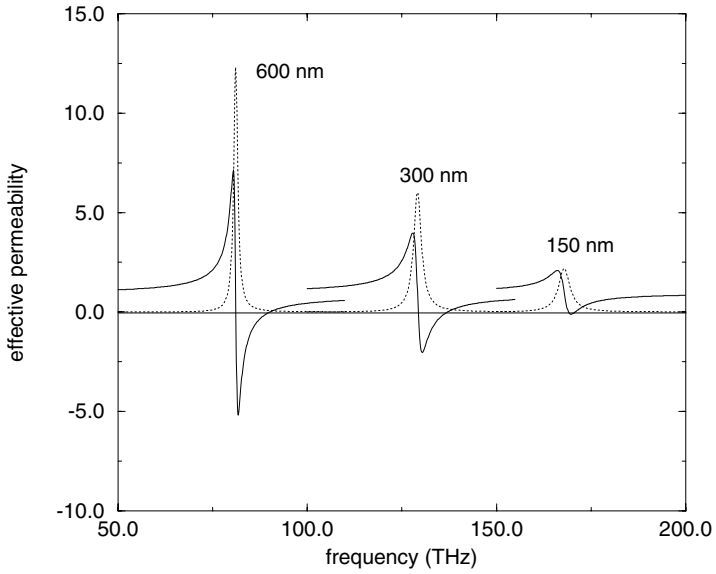

Figure 8. The effective permeability, given by equation (12), of a medium consisting of a square array of the model structures of figure 7. The solid curves are the real parts and the dotted curves are the imaginary parts in each case. The labelling denotes the unit-cell length in nanometres which we consider. The corresponding dimensions of each structure are given in table 2.

An important factor which is not accounted for in our analytic model is the effect of multiple scattering within the metal film which can lead to increased absorption once $d < \delta$. Our original choice of $D = 24$ nm was therefore made in order to maximize the area internal to the structure of figure 1(b) while keeping the additional losses due to multiple scattering to a minimum. Also, as the metallic regions become structured on a smaller scale, the effect of the surfaces will be to decrease the electron mean free path and thus increase the level of absorption above the value for the bulk metal. For silver films the observed values of the optical constants depart from their bulk values once the thickness is <20–30 nm [10].

If we therefore require that $d > \delta$ and that the damping of the resonance should be small, we then require that R should be large in comparison to 2δ. These requirements suggest that in order to increase the operating frequency of these structures we should reduce the capacitance in the structure. This can be achieved by introducing more divisions around the circumference of the ring. Because they are connected in series, the total capacitance is then reduced while leaving the quality factor of the resonance essentially unaltered provided that $d_c \ll R$. Unless the separation d_c is very small however, this procedure will result in the unit-cell dimension and the free-space wavelength at the resonance frequency becoming comparable. In this limit we can no longer consider the crystal as an effectively homogeneous medium.

A final interesting property of these structures is their ability to concentrate the electrostatic energy of the incident field into the small volume between the plates of the capacitors in the structure. This property suggests the potential for enhancing non-linear effects with these structures and for making active structures with very small quantities of the non-linear material.

Following the reasoning outlined in [1] we can arrive at a measure of the enhancement of the energy density in the region between the plates of the capacitors. The electric field in these

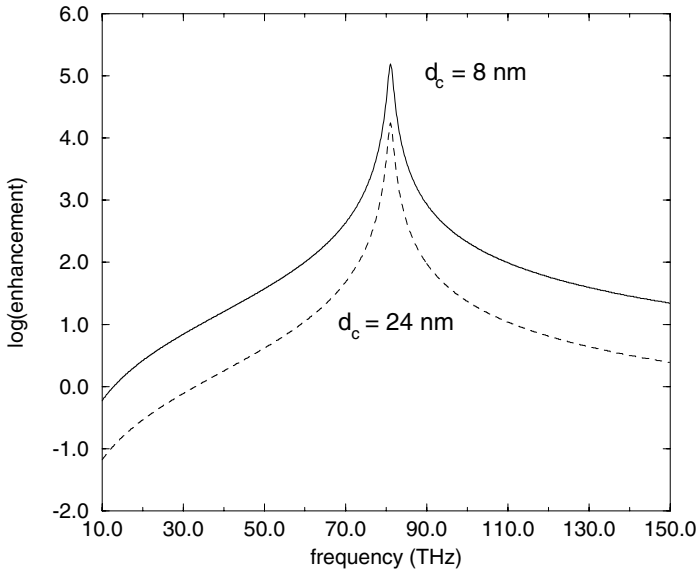

Figure 9. The enhancement of the electrostatic energy density within the gaps in the metallic ring of figure 7 for two values of the separation d_c as indicated.

regions is $E_c = V_c/d_c$ where the voltage across each capacitor, V_c, is given by

$$V_c = \frac{\mathrm{i}dd_c}{\omega\epsilon_0 L_c} j_\phi. \tag{17}$$

Evaluating at the resonance frequency we obtain

$$|E_c| = \frac{Rd}{2\epsilon_0 L_c \delta^2 \gamma} |H_{ext}|. \tag{18}$$

We now assume that the electrostatic energy in the incident field is concentrated in the capacitative regions of the structure. This in turn is related to the incident magnetic energy density. Thus our enhancement factor, Q, for the electrostatic energy density is given by

$$2Q = \frac{(1/2)\epsilon_0 |E_c(\omega_0)|^2}{(1/2)\mu_0 |H_{ext}(\omega_0)|^2} \tag{19}$$

$$Q = \frac{c_0^2}{8}\left(\frac{Rd}{L_c \delta^2 \gamma}\right)^2, \tag{20}$$

where the factor of two arises because the energy is shared between the two capacitative regions in the structure. In figure 9 we have plotted the logarithm of the enhancement factor against the frequency for two configurations of the structure of figure 7(a). The dimensions R and d are the same in each case, being 161.4 and 14.6 nm respectively. The total capacitance is also the same in each case, the ratio L_c:d_c being 144:24 and 48:8 as indicated.

It is evident that these structures have considerable potential for enhancing non-linear effects and for doing so very efficiently. Although the effective permeability calculated using the model is greater than that calculated using the transfer matrix, we can still expect an enhancement in the region of five orders of magnitude provided that the separation d_c is small enough. These levels of enhancement are comparable to those implied by studies of the surface-enhanced Raman scattering for molecules adsorbed on rough surfaces of noble metals [11].

One might expect that because, at the position of the resonance frequency, the peak energies contained in the electrostatic field and in the magnetic field are equal, we should also measure a large dielectric response in the vicinity of the resonance. We found that the key to observing a large magnetic response but a limited dielectric response is to structure the resonator such that the large induced dipole fields screen one another. Examining figure 7(b) it is clear that the induced current distribution is dipolar and thus the averaged magnetic response dominates over the averaged dielectric response which has an underlying quadrupolar symmetry.

Finally, note that this structure displays a magnetic response only when the incident magnetic field is oriented along the axis of the column. For the opposite polarization the electric field will see a continuous conducting path and the crystal will respond in the manner of an effective metal. Thus, creating an isotropic structure would require that we employ planar elements and orient them along all three Cartesian axes. Fabrication of a three-dimensional structure such as this and at submicron scales would represent a very considerable technological challenge.

5. Conclusions

Numerical calculations of the effective permittivity and permeability have been presented for a photonic crystal composed of metallic resonators structured on a nanometric scale. On incorporating a large capacitance and inductance into the structure, the free-space wavelength at the resonance frequency was much larger than the unit-cell dimension and thus the crystal responded in the manner of a homogeneous system with a strongly dispersive magnetic permeability near the resonance frequency. The permeability was found to be negative above the resonance frequency. The smaller level of dispersion in the effective permittivity of the structure was found to be reduced by increasing the separation between the length scales defining the unit cell and the free-space wavelength. A physical model for the effective permeability of the crystal was also derived. This model demonstrates that the inertial inductance of the electrons in the metal represents a barrier to the operation of these structures as effective media in the optical region of the spectrum. We have also shown that these structures provide a means of concentrating the electromagnetic energy of the incident field into very small volumes within the structure. This raises the possibility of creating active structures with very small quantities of non-linear material.

Acknowledgments

Thanks to N Kumar and S Anantha Ramakrishna for helpful discussions.

References

[1] Pendry J B, Holden A J, Robins D J and Stewart W J 1999 *IEEE Trans. Microw. Theory Tech.* **47** 2075
[2] Wiltshire M C K, Pendry J B, Young I R, Larkman D J, Gilderdale D J and Hajnal J V 2001 *Science* **291** 849
[3] Pendry J B, Holden A J, Robins D J and Stewart W J 1998 *J. Phys.: Condens. Matter* **10** 4785
[4] Veselago V G 1968 *Sov. Phys.–Usp.* **10** 509
[5] Shelby R A and Smith D R 2001 *Science* **292** 77
[6] Pendry J B 2000 *Phys. Rev. Lett.* **85** 3966
[7] O'Brien S and Pendry J B 2002 *J. Phys.: Condens. Matter* **14** 4035
[8] Pendry J B and MacKinnon A 1992 *Phys. Rev. Lett.* **69** 2772
[9] Smith D R, Schultz S, Markos P and Soukoulis C M 2002 *Phys. Rev.* B **65** 195104
[10] Johnson P B and Christy R W 1972 *Phys. Rev.* B **6** 4370
[11] García-Vidal F J and Pendry J B 1996 *Phys. Rev. Lett.* **77** 1163